

# Proposal of High Backdrivable Control Using Load-Side Encoder and Backlash

Shota Yamada\*, Hiroshi Fujimoto\*\*

The University of Tokyo

5-1-5, Kashiwanoha, Kashiwa, Chiba, 227-8561 Japan

Phone: +81-4-7136-3873\*, +81-4-7136-4131\*\*

Email: yamada@hflab.k.u-tokyo.ac.jp, fujimoto@k.u-tokyo.ac.jp

**Abstract**—Backdrivability is highly required in various robotic fields such as industrial, welfare, and wearable robots. To miniaturize the system, gear reducers are often used. In gear reducers, there are backlashes, which deteriorate control performance. However, only from the view point of backdrivability, backlash has an ideal characteristic because the load side idles within the backlash width (i.e. When someone put external force at the load side, the load side does not hit the motor side within the backlash width). This means that external forces from the load side only feel the load-side impedance without motor-side impedance. The proposed method uses this idling characteristic to enhance backdrivability. Moreover, in industry, there is a trend toward the expansion of the use of load-side encoders thanks to their cost reduction. Based on this industrial trend, the proposed method is realized using both the motor-side and load-side encoder information to improve backdrivability. Simulation and experimental results demonstrate proposed method's effectiveness.

**Index Terms**—Backdrivability, Backlash, Load-side encoder, Two-inertia system, Impedance control, Force control

## I. INTRODUCTION

Force control is gathering a lot of attentions these days [1]. Industrial robots are used in separated areas surrounded by fences for human safety. To answer demands on building flexible product lines, fenceless robots with force control are being developed actively. Thus, industrial robots are required to work safely with human cooperatively [2]. Since welfare robots are also attracting a lot of attentions, the importance of force control, which makes human-friend motion control possible is expected to increase.

Robots usually have gear reducers to miniaturize the whole systems [3]. For controlling the systems, low resonance frequencies caused by flexible gear reducers restrict their control bandwidths. Conventionally, the systems are modeled as two-inertia systems to consider their resonant characteristics, and a lot of research are conducted aiming at higher control bandwidths [4]. Moreover, gear reducers have not only low stiffness but also nonlinearities such as backlash, which deteriorates the precision of positioning at the load side [5]. Backlash, the gap between teeth in a gear reducer, is known as an element which is difficult to deal with. A lot of research has been published regarding compensation of backlash [6], [7].

To obtain high precise positioning at the load side, the number of devices with high resolution encoders at the load

side is increasing in industry. Also in robots' fields, it is easily expected that their reduction in cost will increase the use of load-side encoders. Therefore, we have developed a new structure robot module with a load-side encoder in reference [8]. Development of novel control methods using load-side encoder information is highly required.

Backdrivability is one of the main concepts in force control. It indicates how easily the devices can be moved from the load side. Backdrivability is essential in wearable robots since it determines how easily wearers can move [9]. The main factors deteriorating backdrivability are motor-side impedance and friction amplified by a gear reducer. By enhancing backdrivability in industrial robots and welfare robots, workers can move the robots easily. Improving backdrivability can also prevent injuring humans and hardware destruction, when robots have collisions with humans [10].

In this paper, by using a setup, which can be modeled as a two-inertia system with backlash, a high backdrivable control method using load-side encoder and backlash is proposed. Although backlash is known to be difficult to deal with, only from the view point of backdrivability, backlash has an ideal



Fig. 1. Outlook of two-inertia system motor bench.

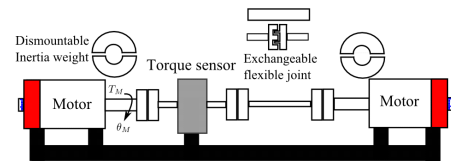


Fig. 2. Structure of the two-inertia system motor bench.

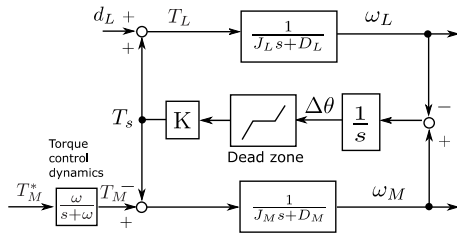


Fig. 3. Block diagram of the two-inertia system motor bench.

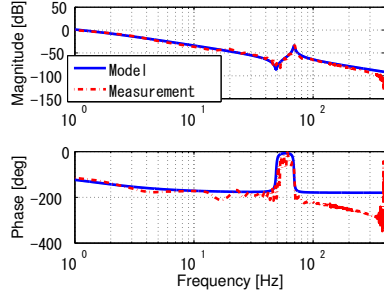


Fig. 4. Frequency responses from the motor-side input current to the motor side angle.

characteristic because the load side idles within the backlash width (i.e. When someone put external force at the load side, the load side does not hit the motor side within the backlash width). This means that external forces from the load side only feel the load-side impedance without motor-side impedance. The proposed method uses this idling characteristic to enhance backdrivability. The proposed method is practical because it is composed of only PD controller. It does not require precise plant parameters or backlash width, and the gains are easy to tune.

This paper is organized as follows. An experimental setup is introduced and modeled in Section II. In Section III, the proposed method is explained in detail. In Section IV and V, control performance of the proposed method is analyzed in simulations and experiments. Finally conclusions are given in Section VI.

## II. EXPERIMENTAL SETUP

An experimental setup consists of a motor bench with 20 bits high resolution encoders. Outlook and a schematic of the setup are shown in Fig. 1 and 2, respectively. To imitate a device with a low resonance mode, a flexible joint can be inserted between two motors. Moreover, by replacing the flexible coupling with a gear coupling, backlash can be added and removed easily.

### A. Modeling

A block diagram of a two-inertia model of the setup is shown in Fig. 3. Let inertia moment, viscosity, torsional rigidity, torque, and angular velocity be denoted as  $J$ ,  $D$ ,  $K$ ,  $T$ , and  $\omega$ , respectively. Subscripts  $M$  and  $L$  indicate motor side and load side, respectively. Also, motor torque command, motor

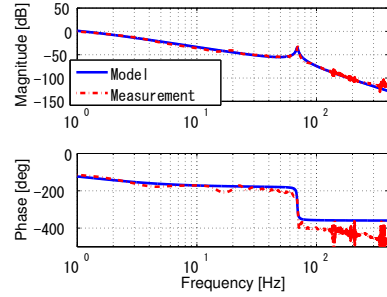


Fig. 5. Frequency responses from the motor-side input current to the load side angle.

TABLE I  
PARAMETERS OF TWO-INERTIA SYSTEM MOTOR BENCH.

Motor-side moment of inertia $J_M$	1.03e-3	kgm <sup>2</sup>
Motor-side viscosity friction coefficient $D_M$	8.00e-3	Nms/rad
Torsional rigidity coefficient $K$	99.0	Nm/rad
Load-side moment of inertia $J_L$	0.870e-3	kgm <sup>2</sup>
Load-side viscosity friction coefficient $D_L$	1.71e-3	Nms/rad

torque, joint torque, load-side torque, and torsional angle are indicated as  $T_M^*$ ,  $T_M$ ,  $T_s$ ,  $T_L$ ,  $\Delta\theta$ . Since the current control system is designed such that the control bandwidth is 1 kHz, the dynamics is expressed as the 1st order low pass filter whose cut off frequency is 1 kHz.

Generally, plants include various nonlinearities such as backlash [5]. In this paper, backlash is modeled as dead zone and an initial value of  $\Delta\theta$  is set as the middle point of dead zone.

Frequency characteristics of the setup from the motor current to the motor-side angle and the load-side angle are shown in Fig. 4 and 5. These figures show that the setup can be modeled as a two-inertia system whose antiresonance frequency is 57 Hz and resonance frequency is 71 Hz. Parameters identified by the fitting are shown in Tab. 1.

### B. Backlash identification

For backlash identification, motor-side velocity control is implemented. As expressed in (1), backlash can be calculated by integrating the torsional angular velocity between  $t_1$ , when the load separates from the motor side and  $t_2$ , when the load contacts the motor side again [11], [12]. Let the dead zone width be  $\pm\epsilon$ .

$$2\epsilon = \left| \int_{t_1}^{t_2} (\omega_M - \omega_L) dt \right| \quad (1)$$

In the experiments, the dead zone width is calculated by not integrating the torsional angular velocity but using the angles at  $t_1$ ,  $t_2$  obtained by the encoders on motor and load sides. Fig. 6 shows a part of the identification experiments. Averaging the results leads to  $\epsilon = 6.0$  mrad.

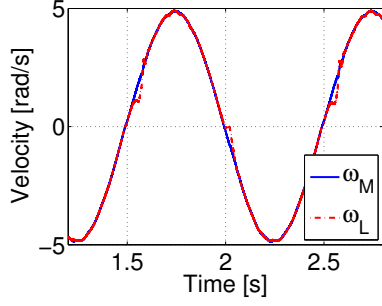


Fig. 6. Experiment for identification of backlash.

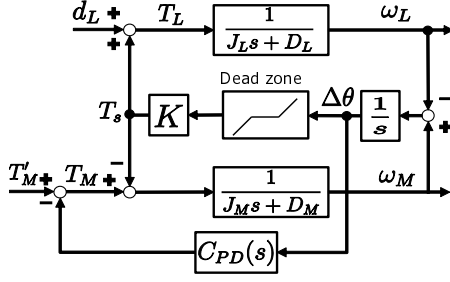


Fig. 7. Block diagram of the proposed method.

### III. PROPOSED METHOD FOR HIGH BACKDRIVABILITY

#### A. Summary of the proposed method

By using load-side encoder information and backlash actively, high backdrivable control is achieved. When human inputs external force from the load side, the load is hard to move because the friction and the impedance of the reducer and the motor are amplified by the gear ratio. Within the backlash width, human feels only the load-side impedance since the load is not connected with the motor. To use this characteristic, when external force is input, the proposed method works such that the motor side follows the load side within the backlash width.

Block diagram of the proposed method is shown in Fig. 7.  $C_{PD}(s)$  indicates PD controller.

#### B. Meaning and Design of PD controller

The proposed method consists of PD control for torsional angle. PD controller for torsional angle adds a virtual spring and a damper between the motor and load side. Although a suppression method for self-excited vibration caused by backlash is proposed by applying P controller for torsional angle in reference [13], a control method for enhancing backdrivability is not proposed yet. Here, a new control input and PD controller gains are denoted as  $T'_M$ ,  $K'$ , and  $K_d$ , respectively. PD controller for torsional angle means that the motor-side angle and angular velocity follow the load-side ones as expressed in (2) when  $T'_M = 0$  (see Fig. 7). Note that initial value of  $\Delta\theta$  is set as the middle point of dead

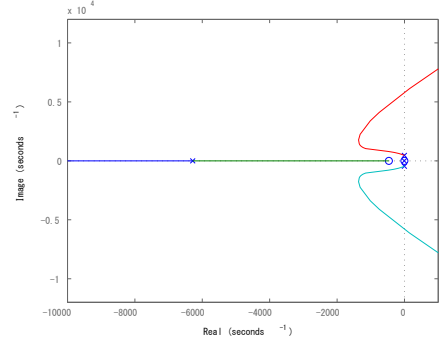


Fig. 8. Root locus in P controller case.

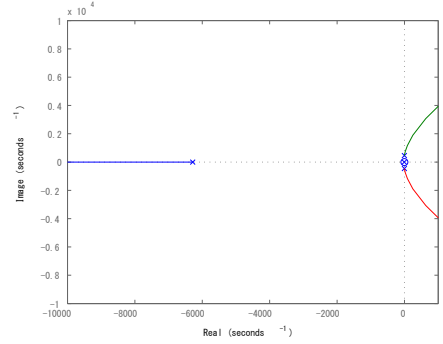


Fig. 9. Root locus in PD controller case.

zone.

$$\begin{aligned} T'_M &= 0 - (K' + K_d s)\Delta\theta \\ &= K'(\theta_L - \theta_M) + K_d(\omega_L - \omega_M) \end{aligned} \quad (2)$$

Without control, the load side has a collision with the motor side by the load-side external force input. The collision excites vibration and deteriorates control performance. With the proposed method, the virtual spring and damper avoid the collision and vibration.

P gain  $K'$  is designed such that torsional angle response by expected maximum external force becomes smaller than the backlash width. Therefore, the only necessary information for designing  $K'$  are rough values of the maximum amplitude of the external force and the backlash width. The D gain  $K_d$  can be tuned such that the torsional angle response has enough damping.

Too high  $K'$  destabilizes resonant poles due to the delay from the current control. The root locus plots in P and PD controller cases are shown in Fig. 8 and 9. Please note that the dead zone model is removed in the root locus analyses. Adding D control action can stabilize the resonant poles and make high  $K'$  design possible.

### IV. SIMULATION

Backdrivability is evaluated by the load-side velocity response when step load-side external force is input from

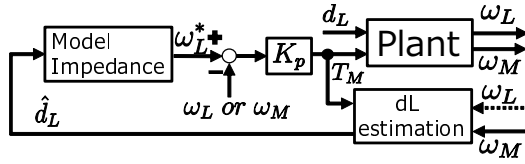
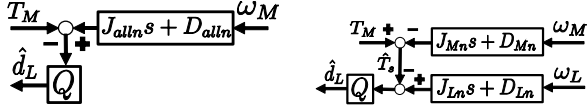


Fig. 10. Block diagram of impedance control.



(a) Rigid body model based DOB. (b) Two-inertia model based DOB.

Fig. 11. Block diagram of force estimation by DOB.

0.050 s to 0.25 s. For performance comparison, impedance controller is implemented as a conventional method. To feel only the load-side impedance, model impedance in impedance controller is designed such that it coincides with the load-side impedance. Other detail conditions are explained in the last section of this chapter.

#### A. Impedance control (Conventional methods)

The most common method to enhance backdrivability is impedance control. Desired impedance is achieved by velocity FB control with the velocity reference generated by the model impedance  $1/(J_{model}s + D_{model})$ . In this paper, a velocity P controller with gain  $K_p$  is applied. Block diagram of impedance control for a two-inertia system is shown in Fig. 10. Here,  $\hat{d}_L$  and  $\omega_L^*$  indicates estimated external force and load-side velocity command value, respectively.

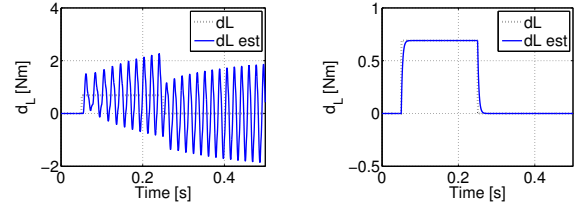
1) *Estimation with rigid body model*: Impedance control requires the detection or estimation of the external force  $d_L$ . In this paper, DOB is applied to estimate the external force. Firstly, the simplest rigid body model expressed as (3) is used for estimation. Subscript  $n$  indicates nominal value.

$$P_{all}(s)^{-1} = J_{alln}s + D_{alln} \quad (3)$$

$$J_{alln} = J_{Mn} + J_{Ln}, \quad D_{alln} = D_{Mn} + D_{Ln}$$

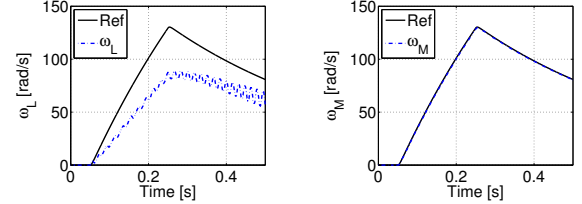
Block diagram is shown in Fig.11(a). Here,  $Q$  is the 1st order low pass filter to realize DOB. Fig.12(a) shows a simulation result of the estimation. The estimated value has large vibration because the estimation model does not consider two-inertia resonant characteristic.

2) *Estimation with two-inertia model*: To consider two-inertia resonant characteristic, double DOB using both motor and load side encoder information is applied [14]. Block diagram is shown in Fig. 11(b).  $d_L$  can be precisely estimated as shown in Fig. 12(b). Although impedance control is realized by feedback of  $\omega_L$ , velocity response does not follow the reference precisely as shown in Fig. 13(a) because it is impossible to have enough high gain  $K_p$ . This is because non-collocated load-side information has a large phase lag and it restricts control bandwidth.



(a) Response of rigid body model based DOB. (b) Response of two-inertia model based DOB.

Fig. 12. Force estimation by DOB.



(a)  $\omega_L$  in  $\omega_L$  FB impedance control. (b) Velocity reference and  $\omega_M$  in the conventional method 1.

Fig. 13. Velocity responses in the conventional method.

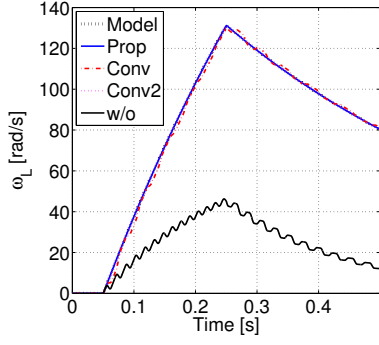
To avoid this non-collocated problem, collocated  $\omega_M$  is fed back instead of  $\omega_L$ . Simulation results of  $\omega_L^*$  and  $\omega_M$  are shown in Fig. 13(b).  $\omega_M$  follows  $\omega_L^*$  precisely. This method is defined as the conventional method 1 and compared with the proposed method.

3) *Measurement with sensor*: DOB cannot estimate  $d_L$  precisely with modeling errors.  $d_L$  can be measured by a force sensor instead of applying DOB. This method is defined as the conventional method 2. Please note that this method does not require a load-side encoder but requires a external force sensor.

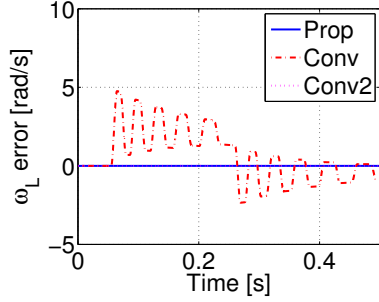
#### B. Comparison in simulations

$\omega_L$  responses are shown in Fig.14(a). A legend "Model" is used as a reference because it indicates the response when the plant model is only  $1/(J_Ls + D_L)$ . Fig.14(b) shows the error from the model response. Without control,  $\omega_L$  is not increased much and it has vibration. The responses of the other methods follow the model response precisely, which means backdrivability is improved and impedance of the whole system coincides with the load-side impedance. Fig.14(b) shows there is an error in the conventional method 1. This is because  $K_p$  cannot be increased high enough due to the DOB delay.

Fig.15 shows that the torsional angles stay within the backlash width in the proposed method and the conventional method 2 while in the conventional method 1 it does not. The joint torque  $T_s$  should be 0 because the model impedance equals to the load-side impedance. However,  $T_s$  shown in Fig. 16(a) in the conventional method 1 does not keep 0 due to the collision between the load and motor sides. From the view point of the external force  $d_L$ ,  $T_s$  works as a disturbance. Therefore, the load-side torque  $T_L$  shown in Fig. 16(b) does not coincide with the input  $d_L$ , which leads to the errors of



(a)  $\omega_L$  responses.



(b)  $\omega_L$  errors from the model response.

Fig. 14. Comparison of  $\omega_L$  responses in simulation.

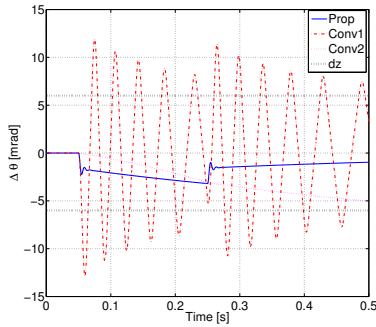


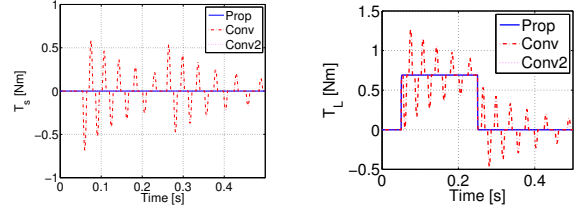
Fig. 15.  $\Delta\theta$  responses in simulation.

$\omega_L$ .

### C. Relationship between the proposed and conventional methods

In the conventional methods,  $\omega_L^*$  is generated with the model impedance, and then  $\omega_M$  is fed back and controlled with P controller. Therefore, when the model impedance coincides with the load-side impedance without any errors, the conventional methods correspond to the proposed method with P gain  $K' = 0$ . In the proposed method, the system can have high rigidity thanks to P control, which can avoid the collision between the load and motor sides. The proposed method corresponds to PI-based velocity impedance control when there is no modeling error.

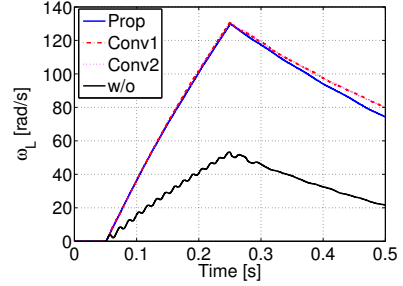
The proposed method has two clear advantages over the



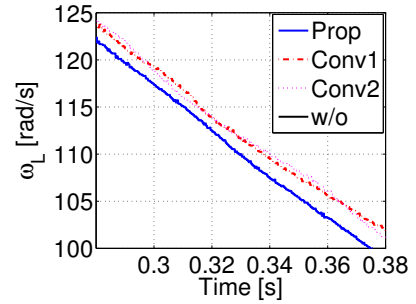
(a)  $T_s$  comparison.

(b)  $T_L$  comparison.

Fig. 16. Comparison of Joint torque and load-side torque responses.



(a)  $\omega_L$  responses.



(b) Zoom of Fig. 17(a).

Fig. 17.  $\omega_L$  comparison in experiments.

conventional impedance control: no need to measure or estimate external forces, and ease of implementation. The proposed method does not require a force sensor, DOB, or precise plant parameters. Therefore, when there is no need to change the load-side impedance, the proposed method should be applied to enhance backdrivability.

### D. Simulation conditions

In simulations, there is no modeling errors. Step reference is filtered with the 1st order low pass filter whose cut off frequency is 500 Hz. Pseudo differential in PD controller is implemented with a 1st order low pass filter whose cut off frequency is 1 kHz. The cut off frequency of Q is designed as 30 Hz.

## V. EXPERIMENTS

In the experiments, since  $d_L$  is input by the load-side motor, the torque reference of the load-side motor is used as  $d_L$  in the conventional method 2. To make the same conditions as in simulations, initial motor-side angle is set in the middle of the backlash by position control. Please note that the

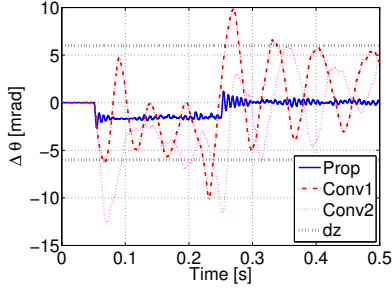


Fig. 18.  $\Delta\theta$  responses in experiments.

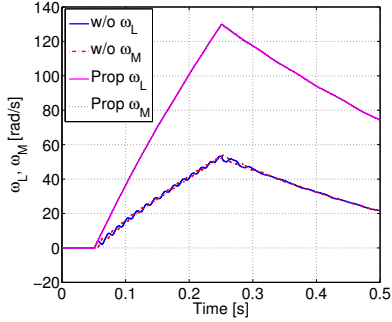


Fig. 19. Comparison of  $\omega_M$  and  $\omega_L$  in experiments.

conventional method 2 cannot have high  $K_p$  due to the noise in measurement values and the dead time. Therefore, its gain is almost same as the gain in the conventional method 1.

Fig. 17(a) shows the comparison of  $\omega_L$  responses. The experimental results are similar to the simulation ones. There is a difference between the proposed method and the conventional methods because the designed model impedance does not coincide with the plant's load-side impedance due to the modeling error. Fig. 17(b) is a magnified figure from 0.28 s to 0.38 s. The proposed method shows better performance while the conventional methods have vibration because they cannot have high  $K_p$ .

Torsional angle responses are shown in Fig. 18. The proposed method can suppress  $\Delta\theta$ , while the conventional methods cannot keep  $\Delta\theta$  within the backlash width, which deteriorates the  $\omega_L$  responses.

Finally, Fig. 19 shows the comparison of  $\omega_M$  and  $\omega_L$  responses between with and without the proposed method. Without control,  $\omega_M$  and  $\omega_L$  responses have 180-degree phase difference caused by the resonance, while in the proposed method  $\omega_M$  corresponds to  $\omega_L$  because the motor side follows the load side by adding a virtual spring and damper.

## VI. CONCLUSION

Based on the trend of increasing load-side encoders, high backdrivable control using load-side encoder information and backlash is proposed. Although backlash is known to be difficult to deal with, only in terms of backdrivability, backlash has an ideal characteristic. The proposed method uses the backlash

characteristic that the load side idles in the backlash width. The proposed method consists of only one PD controller and its advantages are verified in simulations and experiments.

The proposed method can remove the motor-side impedance and friction effects. However, it cannot change the load-side impedance arbitrarily. Therefore, extension of the proposed method to assist the load side will be studied in the future.

## VII. ACKNOWLEDGMENTS

The contributions of DMG MORISEIKI Co., Ltd. are gratefully acknowledged. This project was supported by JSPS and NRF under the Japan – Korea Basic Scientific Cooperation Program. This project was also supported by JSPS KAKENHI Grant Number 16J02698.

## REFERENCES

- [1] T. Yoshioka, A. Yabuki, Y. Yokokura, K. Ohishi, T. Miyazaki, and T. T. Phuong: "Stable Force Control of Industrial Robot Based on Spring Ratio and Instantaneous State Observer", *IEEJ Journal of Industry Applications*, Vol. 5, No. 2, pp. 132–140, (2016).
- [2] G. B. Avanzini, N. M. Ceriani, A. M. Zanchettin, P. Rocco, and L. Bascetta: "Safety Control of Industrial Robots Based on a Distributed Distance Sensor", *IEEE Trans. Control Systems Technology*, Vol. 22, No. 6, pp. 2127–2140, (2014).
- [3] K. Kong, J. Bae, and M. Tomizuka: "A Compact Rotary Series Elastic Actuator for Human Assistive Systems", *IEEE Trans. on Mechatronics*, Vol. 17, No. 2, (2012).
- [4] K. Yuki, T. Murakami, and K. Ohnishi: "Vibration Control of 2 Mass Resonant System by Resonance Ratio Control", *Industrial Electronics Society Annual Conference (IECON-1993)*, pp. 2009–2014, (1993).
- [5] M. Iwasaki, M. Kainuma, M. Yamamoto, and Y. Okitsu: "Compensation by Exact Linearization Method for Nonlinear Components in Positioning Device with Harmonic Drive Gearings", *Journal of JSPE*, Vol. 78, No. 7, pp. 624–630, (2012).
- [6] M. Nordin and P. Gutman: "Controlling mechanical systems with backlash – a survey", *Automatica*, Vol. 38, pp. 1633–1649, (2002).
- [7] D. K. Prasanga, E. Sariyildiz, and K. Ohnishi: "Compensation of Backlash for Geared Drive Systems and Thrust Wires Used in Teleoperation", *IEEJ Journal of Industry Applications*, Vol. 4, No. 5, pp. 514–525, (2015).
- [8] S. Yamada, K. Inukai, H. Fujimoto, K. Omata, Y. Takeda, and S. Makinouchi: "Joint torque control for two-inertia system with encoders on drive and load sides", *Proc. of the 13th IEEE Int. Conf. on Industrial Informatics (INDIN)*, pp. 396–401, (2015).
- [9] B. Na, J. Bae, and K. Kong: "Back-drivability recovery of a full lower extremity assistive robot", *Proc. of the 12th International Conference of IEEE on Control, Automation and Systems (ICCAS)*, pp. 1030–1034, (2012).
- [10] Y. Kuroki, Y. Kosaka, T. Takahashi, E. Niwa, H. Kaminaga, and Y. Nakamura: "Cr–N Alloy Thin-film Based Torque Sensors and Joint Torque Servo Systems for Compliant Robot Control", *IEEE International Conference on Robotics and Automation (ICRA-2013)*, pp. 4954–4959, (2013).
- [11] S. Villwock and M. Pacas: "Time-Domain Identification Method for Detecting Mechanical Backlash in Electrical Drives", *IEEE Trans. Ind. Electron.*, Vol. 56, No. 2, (2012).
- [12] K. Yuki, T. Murakami, and K. Ohnishi: "Study of on-line backlash identification for PMSM servo system", *Proc. of the 38th annual conference on IEEE Industrial Electronics Society (IECON)*, pp. 2036–2042, (2012).
- [13] K. Mochizuki and I. Awaya: "Vibration suppression control for mechanical systems with backlash using describing function and model-matching method", *The Japan Society of Mechanical Engineers, Dynamics and Design Conference*, No. 745, (2014).
- [14] C. Mitsantisuk, M. Nandapaya, K. Ohishi, and S. Katsura: "Design for Sensorless Force Control of Flexible Robot by Using Resonance Ration Control Based on Coefficient Diagram Method", *Automatika*, vol. 54, no. 1, pp. 62–73, (2013).